Impact of post-synthetic treatments on unidirectional H-ZSM-22 zeolite catalyst: Towards improved clean MTG catalytic process

Pablo del Campo[a], Unni Olsbye[a], Karl Petter Lillerud[a], Stian Svelle[a*] and Pablo Beato[b**]

[a]*SMN Centre for Materials Science and Nanotechnology, Department of Chemistry, University of Oslo, N-0315 Oslo, Norway*

[b]*Haldor Topsøe AS, Nymøllevej 55, DK-2800 Kgs. Lyngby, Denmark*

* Corresponding author. Tel.: +47 22 85 54 54 ; fax: +47 22 85 54 41

** Corresponding author. Tel.: +45 45 27 20 00; fax: +45 45 27 29 99

E-mail addresses: stian.svelle@kjemi.uio.no (S. Svelle), pabb@topsoe.dk (P. Beato)

Abstract

In the present study, a series of H-ZSM-22 mesoporous catalysts resulting from three different desilication treatments (NaOH treatment, treatment using mixtures of NaOH/CTAB and using mixtures of NaOH/TBAOH) and sequential acid leaching over two different (commercial and lab-made) microporous ZSM-22, were tested in the conversion of methanol to hydrocarbons. The influence of the post-synthetic treatments on the catalytic lifetime and product distribution was examined. The influence of the starting catalysts on the change in the catalyst properties was also reflected in the catalytic behaviour. An increase of about 11 times in lifetime and 10 times in total methanol conversion capacity with respect to the untreated catalyst was reached after the CTAB/NaOH and acid treatment over the commercial material, whereas an extension of lifetime by more than 30 times reflected in a 17-fold increase in conversion

capacity was achieved for the lab-made catalysts treated with NaOH and acid. The yield towards the aromatic-free C_{5+} alkene fraction was optimized after the post-synthetic treatments, up to 58 % of products meeting clean gasoline requirements. The correlations between porosity, acidity and total conversion capacity suggested a more efficient use of the hierarchical catalyst particle as a result of a synergetic effect of mesopore formation, enhanced accessibility to the micropores and acid sites, and increased adsorption and transport properties. Mechanistic information extracted from the analysis of the C_3/C_2 and ethene/2M2B ratios, suggested that the improved catalyst properties allow a longer propagation of the olefin cycle with reaction time.

Keywords

Methanol-to-hydrocarbons

Zeolite catalyst H-ZSM-22

Post-synthetic

Hierarchical

Olefin cycle

1. Introduction

The conversion of methanol to hydrocarbons (MTH) constitutes the last stage of the route to produce high-value petrochemical products from low valuable feedstock as natural gas, coal or biomass via syngas [1-3], and represents a real alternative to the most used processes which exploit the dwindling global oil reserves to produce energy carriers [4]. The MTH reaction proceed over acidic zeolite or zeotype materials, known as shape selective catalysts, since they are able to discriminate reactants, products and reaction intermediates based on their molecular size [5]. The acid sites responsible for

the methanol conversion are located inside the pores and channels of the zeolite crystal and catalyse the multiple reactions of the MTH process, which can be tuned to produce gasoline-rich or olefin-rich products by choosing the appropriate catalyst architecture, composition and reaction conditions [2, 6, 7]. Currently, with the rise of oil prices, intense commercialization efforts are ongoing for ZSM-5 based methanol to gasoline (MTG) and SAPO-34 based methanol to olefins (MTO) technologies [1].

The major drawback of the existing ZSM-5 based MTG process is the content of carcinogenic aromatic compounds in the produced gasoline, which is high considering the environmental restrictions on the composition of transportation fuels. However, recent investigations have shown that this problem can be surpassed by using H-ZSM-22 as the active catalyst for the process. The ZSM-22 zeolite with TON topology has a one directional pore structure comprising non-intersecting 10-ring channels [8]. Due to this specific pore architecture, it possess unique shape selective properties and is able to selectively yield a product mixture that is intermediate to that found for SAPO-34 and ZSM-5, being rich in C_{5+} branched alkanes and alkenes and virtually without aromatics [9]. The mechanistic interpretation is based on the fact that the aromatic molecules only participate in one of the cycles of the MTH dual cycle mechanism and, by using H-ZSM-22, the aromatic cycle can be suppressed, thus producing a product virtually free of aromatics [2, 10, 11]. Therefore, the H-ZSM-22-based MTH product might meet the present fuel demands and might be suitable as gasoline after hydrogenation. Alternatively, the alkene rich product might be utilized as an alkylation feedstock to increase the carbon number and provide saturation. Currently, however, the process is far from becoming a commercial reality, owing the short lifetime or rapid deactivation by coke deposition, resulting in a limited methanol conversion capacity for the H-ZSM-22 catalyst [2, 9].

Since H-ZSM-22 has one-directional non-interconnected channels, its acid sites are only accessible by the rare ends of the crystals. Th gives rise to molecular transport limitations within the zeolite micropores. This weakness can be overcome by introducing a secondary network of pores within the existing micropore system of the zeolite, i.e. producing mesoporous zeolites. As pointed out by the numerous literature reviews, several synthetic approaches have been developed to overcome the diffusion limitations and to obtain improved catalysts for different processes [12-19]. The so-called hierarchical materials have shorter diffusion pathways for the reaction intermediates and products and allow catalytic reactions proceed on the mesopore surface and in the pore mouths. Concerning the MTH reaction, most of the research has been dedicated to obtain mesoporous ZSM-5 zeolites by desilication with alkaline treatment [20, 21], surfactant-assisted solutions [22-24], or different processes [25, 26]. The general effect of the mesoporosity is an increased lifetime. This is attributed to a more efficient use of the catalyst crystal which results in an increased resistance towards coking, lower rates of coke formation or formation of coke species mainly on the external surface of the catalyst. Additionally, a significant increase in the propene and C_{5+} selectivities was demonstrated in MTG or MTO studies over ZSM-5 [20, 26]. The influence of the connectivity and location of the mesopores, side effects, and acidity modifications on the catalytic properties is, however, still under debate [26-28].

Intuitively, the introduction of mesoporosity lead to a superior catalytic performance for zeolites which are more predisposed to suffer from diffusion limitations, such as one-dimensional systems with medium sized pores. This has been demonstrated with TON zeolite catalysts in isomerization and cracking reactions, for which pore mouth catalysis plays a significant role [29-33]. However, to the best of our knowledge, very few studies compare mesoporous and microporous H-ZSM-22 catalysts in the MTG

reaction. We have previously conducted time- and space-resolved high energy operando XRD measurements to evaluate differences in activity and deactivation behaviour between two such catalysts during MTH reaction [34]. In a very recent study, Dyballa *et al.* focused on the MTO conversion over mesoporous ZSM-22 zeolite synthesized by alkaline desilication and subsequent acid treatment [35]. It was found thatthe lifetime was enhanced by a factor of 2 for the mesoporous catalysts with an optimal Brønsted acidity, accompanied by a highest propene selectivity of 48 %. Furthermore, the product spectrum obtained for the purely microporous and the mesoporous catalyst was very similar, suggesting that the 10-ring pore system governs the shape selective properties of the H-ZSM-22 catalyst in MTO.

An extensive characterization study of mesoporous ZSM-22 zeolites prepared from two different parent materials by three different desilication approaches (using NaOH, mixtures of CTAB/NaOH and mixtures of TBAOH/NaOH), followed by acid leaching is presented in the complementary article [X]. The decisive effect of the morphology of the starting material and of the different desilication agents on the mesopore creation, and also the need of the acid washing step to improve the accessibility to the acidic sites in the zeolites were highlighted. In this contribution, we investigate the MTG catalyst performance of the same materials. Two different H-ZSM-22 samples were used as starting materials with the aim to correlate the properties of the starting material with the resulting catalyst performance seen for the treated material. One catalyst sample derived from each post-synthetic approach was chosen, based on its superior porous and acidity features. First, we will recapitulate the most relevant results from the characterization study. Second, the changes in catalyst lifetime and product distribution will be examined. In the last part of this contribution, we aim to elucidate the causes of the significant improvement in catalyst performance observed for the hierarchical

catalyst by analysing the porosity and acidity features and also the diffusion properties and degree of accessibility to the microporevolume and acid sites.

2. Experimental Section

2.1. Catalyst preparation

In this study, two microporous H-ZSM-22 catalyst samples will be compared with their desilicated and acid-washed (mesoporous) counterparts. The parent commercial H-ZSM-22 (supplied by Zeolyst International) and the lab-made H-ZSM-22 (synthesized following the procedure described elsewhere [9]) catalysts are coded *c*-ZSM-22 and *m*-ZSM-22, respectively. The mesoporous zeolites were prepared by three desilication approaches, described previously in the complementary article. The same sample codes will be used throughout the present work. For clarification, the post-synthetic treatments and sample codes are summarized in Table S1, and comprises: treatment with NaOH (0.2 M, 80 °C, 2 h, 33 g of zeolite per liter of solution), treatment with a mixture of NaOH/CTAB (0.25 M NaOH and 0.05 M CTAB, 80 °C, 24 h, 50 g l^{-1}), and treatment with a mixture of NaOH/TBAOH (0.12 M NaOH and 0.08 M TBAOH, 65 or 80 °C, 0.5 h, 30 g l^{-1}). Each desilication approach was followed by acid washing in HCl (0.1 M, 65 °C, 6 h, 10 g l^{-1}). The treated materials are coded with the suffix *-at1-HCl*, *-ats1-HCl* and *-tba1(2)-HCl*, respectively. The parent commercial zeolite was also treated with HCl at the same conditions (*c*-ZSM-22-*HCl*), for comparative purposes. All the zeolites were ion exchanged with 1 M NH_4NO_3 solution for 3 x 2 h at 75 °C, followed by calcination in static air at 550 °C for 2 h to obtain the protonated form.

2.2. Characterization methods

The crystallinity and purity of the catalysts were checked with PXRD. The Si/Al ratio was determined by elemental analysis using an MP-AES instrument. The size and morphology of the zeolite particles were analysed by TEM. The surface area, pore volume and pore size distribution were determined from N_2 physisorption. The amount of oxidable coke of the spent catalysts was analysed by TGA. The nature and accessibility of acid sites were investigated using FTIR spectroscopy with CO and pyridine as probe molecules. The accessibility and diffusion properties were investigated with time-dependent uptake of toluene monitored by IR. Experimental details are given in the Supporting Information.

2.3. Catalytic testing

All the catalytic tests were performed at ambient pressure using 50 mg of sample in a fixed-bed quartz reactor with 10 mm outer diameter, 7 mm inner diameter. The protonated zeolite was pressed into wafers, crushed and sieved to obtain particles in the 250-420 μm range. Before each catalytic experiment the samples were calcined in situ in a flow of pure oxygen at 550 °C for 1 hour. Methanol (BDH Laboratory Supplies, >99.8%) was fed by passing He through a saturation evaporator kept at 20 °C (p_{MeOH} = 130 mbar). Catalytic tests were performed at 400 °C and a weight hourly space velocity (WHSV) of 2 g feed per g catalyst per hour. The product stream was analysed online using an automatic injection Gas Chromatograph (GC) connected to the reactor outlet by a heated transfer line. An Agilent 6890N Gas Chromatograph with FID, equipped with a HP-PLOT Q capillary column (15 m, 0.320 mm i.d. film thickness 20 μm) was used for the analysis. The temperature of the GC oven was programmed between 90 and 270 °C with a heating rate of 20 °C/min (hold time of 5 min at 90 °C and at 220 °C and 9 min at 270 °C).

Methanol conversion (*X*), product selectivity (*S*) and product yield (*Y*) were calculated from GC-FID areas, following formulas 1-3 shown below. Methanol and dimethyl ether (DME) were considered as reactants, while all effluent non-oxygen hydrocarbons (HC) were considered reaction products. Appropriate response factors were used for the integrated peak areas for methanol and DME. No correction was employed for the integrated peak areas for the hydrocarbons.

$$X_i(\%) = \frac{area\ of\ HC\ product\ peaks}{total\ corrected\ peak\ area} \times 100 \qquad (1)$$

$$S_i(\%) = \frac{area\ of\ HC\ product\ peak\ i}{total\ area\ of\ HC\ product\ peaks} \times 100 \qquad (2)$$

$$Y_i(\%) = \frac{area\ of\ HC\ product\ peak\ i}{total\ corrected\ peak\ area} \times 100 \qquad (3)$$

3. Results and discussion

3.1. Catalysts under study

Among the extensive amount of samples investigated in the complementary article, one acid washed sample from each desilication approach for each of the two microporous ZSM-22 starting materials were selected for the present catalytic study. In this section, we will summarize the most relevant results extracted from the dedicated synthesis/characterization manuscript [X]. The properties of the parent and treated samples are summarized in Table 1 and the relevant figures are given in the Supporting Information.

Both the two parent materials consist of highly crystalline TON framework, as evidenced by PXRD. TEM micrographs show that the commercial parent (*c*-ZSM-22) catalyst consists of agglomerated rod-like crystals up to 200 nm in width, whereas the lab-made parent (*m*-ZSM-22) catalyst is formed by thinner 30-60 nm nanorods. The N_2 isotherms confirm the microporous character of both untreated catalysts, but also show a higher external pore volume for *m*-ZSM-22, most likely due to the inter-crystalline space formed between aggregated nanocrystals. As expected from the higher aluminium content seen for the *m*-ZSM-22 catalyst (Si/Al ratio of 38 compared to 49 for the *c*-ZSM-22), a taller band corresponding to Brønsted acid sites (BAS) is seen in the FTIR spectra. However, the concentration of Brønsted sites quantified by FTIR of adsorbed pyridine is the same for both samples. This suggests that there are defects or extra framework material in the m-ZSM-22 sample, preventing the diffusion of the pyridine probe molecule through the unidirectional channel system.

After the post-synthetic treatments the following observations are made:

- Preserved crystallinity, as confirmed by PXRD.
- Decrease in the Si/Al ratio after desilication, indicative of a selective removal of Si. This is followed bya restoration to the initial values after the acid treatment, demonstrating that EFAl species were formed upon desilication, and that these are eventually washed out of the crystal by acid leaching.
- Improved textural properties as a result of different modes of mesopore generation, revealed by the N_2 adsorption isotherms. The formation of intra-crystalline mesopores in the commercial crystals was evidenced from the increased surface area, the mesopore size distribution (BJH) and TEM analysis. The NaOH treatment resulted in irregular mesopores and partial crystal dissolution, whereas more defined mesopores (2-3 nm or 2-10 nm in diameter) were generated upon the addition of

CTAB or TBAOH to the alkaline solution, respectively. On the other hand, for the lab-made nanorods, mainly crystal dissolution along boundaries occurred upon desilication, resulting in higher mesopore volume and surface area, together with enhanced microporosity, with the exception of the *m*-ZSM-22-*ats1-HCl* sample.

- Restoration of the total acidity and a minor modification of the Brønsted acidity and formation of Lewis acid sites. For the *m*-ZSM-22-*ats1-HCl* catalyst, severe blocking of the access to the BAS was seen, and for *m*-ZSM-22-*tba1-HCl*, partially blocked access was seen with IR and pyridine.
- A substantial increase in the concentration of surface silanol groups, associated to increased external surface, as seen from the IR analysis of the dehydrated samples.
- Nearly the same acid strength for all the catalysts, as determined by the frequency shift of about $\Delta\nu$ = 325 cm^{-1} seen for the Brønsted band due to OH-CO interaction upon CO adsorption (Fig. S5).

It should be mentioned that, due to limitations in the amount of the *c*-ZSM-22-*ats1-HCl* sample, additional characterization (TGA and toluene uptake experiments) had to be performed with the most similar sample, a zeolite treated with 0.5 M NaOH and 0.05 M CTAB at the same conditions (*c*-ZSM-22-*ats2-HCl*). Therefore, we decided to include the catalytic data of both samples in this work and perform qualitative discussions between them, having confidence that the use of two slightly different samples will not have significant influence on the conclusions made.

3.2. MTH catalytic performance

The causes of the different catalytic behaviour will be analysed in Section 3.3, and a description of the catalytic performance for the untreated and mesoporous catalysts is presented in this section.

3.2.1. Influence on the lifetime

The parent and treated zeolite catalysts were tested in the MTH reaction at identical conditions of 400 °C and WHSV ≈ 2 $gg^{-1}h^{-1}$. Figure 1 shows the methanol conversion versus time on stream for the studied materials. The insets highlight the performance during the first 90 minutes on stream.

The two microporous catalysts (*c*-ZSM-22 and *m*-ZMS-22) displayed a lifetime of nearly 3 h until complete deactivation. Relevant investigations on H-ZSM-22 catalysts have shown a maximum lifetime of 5 h at similar reaction conditions to those of this work [9], or 8 h if the H-ZSM-22 catalyst was tested at 450 ^{o}C and WHSV of 0.5 h^{-1} [35].

Clearly, the post-synthetic treatments enhanced both the initial activity, as shown in the insets in Fig. 1, and the lifetime with respect to the parent H-ZSM-22 catalysts. The small variations in the initial activities were expected from the similar acid site densities (or Si/Al ratios) of the hierarchical catalysts with respect to the microporous starting materials. The time at which the methanol conversion decreases to 50 % ($t_{1/2}$, dashed line in Fig. 1) is used as an indicator of the catalytic lifetime. The surfactant treated catalyst (*c*-ZSM-22-*ats1-HCl*) showed the greatest increase in lifetime among the commercial catalysts, reaching 50 % conversion at approximately 17 hours on stream, which represents an increase by a factor of 11 with respect to the untreated catalyst. The catalyst treated with NaOH (*c*-ZSM-22-*at1-HCl*) also displayed a notable increase in lifetime by a factor of 7, very similar to that seen for the high concentration surfactant treated catalyst (*c*-ZSM-22-*ats2-HCl*). The TBAOH treatment (*c*-ZSM-22-*tba2-HCl*) had a modest influence in lifetime, but still showed appreciable conversions for 5 hours, which is a three-fold increase from the lifetime of the untreated catalyst.

It may be noted that the acid washing of the untreated commercial catalyst (*c*-ZSM-22-*HCl*) had no evident influence on the catalytic lifetime. This result highlights that, not only the acid washing, but the sequential desilication and acid leaching is necessary to improve the catalytic performance of the microporous H-ZSM-22 catalyst. With respect to the lab-made series, the largest increase in lifetime, by a factor of more than 30, to reach $t_{1/2}$ = 16.7 hours, was evidenced for the catalyst treated with NaOH (*m*-ZSM-22-*at1-HCl*). An improvement of about 7 hours was achieved for the catalyst treated with TBAOH (*m*-ZSM-22-*tba1-HCl*), whereas the surfactant treated catalyst (*m*-ZSM-22-*ats1-HCl*) showed a limited increase in lifetime.

Recent studies have demonstrated that a lifetime of approximately 12 hours can be reached until complete loss of activity of hierarchical H-ZSM-22 catalysts with a Si/Al ratio of 34 at 450 °C and WHSV of 0.5 h^{-1} [35]. Noteworthy, the most stable hierarchical catalysts tested here at higher WHSV (*c*-ZSM-*22-ats1-HCl* and *m*-ZSM-22-*at1-HCl*) had a lifetime of approximately 20 hours before complete deactivation, which represents a remarkable improvement over any previously published data [35]. The results also show that the trends in increased lifetime are somehow opposite for the two parent H-ZSM-22 catalysts, suggesting that the influence of the starting catalysts on the change in the catalyst properties derived from the complementary article may also be reflected in the catalytic behaviour.

The untreated commercial (*c*-ZSM-22) catalyst exhibited a short active period followed by a rapid deactivation, in line with previous studies [9]. The lab-made (*m*-ZSM-22) catalyst deactivates more rapidly, which is consistent with the low micropore volume and surface area of this sample (Table 1). The commercial treated catalysts displayed a deactivation profile with slower deactivation rates until they reach $t_{1/2}$, and comparable rapid deactivation after the breakthrough of methanol (Fig. 1a). This behaviour is

proposed to occur when methanol is strongly involved in reactions leading to deactivation by coke [36]. On the other hand, different deactivation profiles can be observed for some of the treated catalysts (Fig. 1b). The surfactant treated catalyst (*m*-ZSM-22-*ats1-HCl*) showed a progressive reduction of methanol conversion with time on stream as the product concentration decreases, which may be indicative of a different deactivation mechanism, in which the coke is formed mainly from the reaction products [36, 37]. The *m*-ZSM-22-*tba1-HCl* catalyst showed an intermediate behaviour, which suggest a contribution of both methanol and reaction products to the coke formation.

The observation that coke is formed mainly from methanol has been previously evidenced by structure-activity correlations derived from time- and space-resolved high energy XRD *operando* studies over *c*-ZSM-22 and hierarchical *c*-ZSM-22-*ats1-HCl* catalysts [34]. Apart from the origin of coke; its location, type and amount may also affect the mode of catalyst deactivation [21, 22, 25, 36, 37]. The total amount of oxidable coke in the spent catalysts was determined by TGA, and the data is presented in Fig. 2. No significant differences were observed in the total coke content, as calculated from the mass loss (%) after burning all the coke deposits from the spent commercial (Fig. 2a) or lab-made catalysts (Fig. 2b). This means that the selectivity towards coke is higher for the untreated materials. Likewise, the temperature at which the carbonaceous species start to burn off was rather similar (close to 340 °C) for all the samples. The similar stability of the coke species suggests no differences on the location or type of the carbonaceous species. This observation would be in-line with the assumption of methanol being the main source of coke species for all samples in this series. The fact that similar type and amount of coke is found for the microporous and micro-/mesoporous spent catalysts combined with the observed slower coking rate/lower coke selectivity for the hierarchical catalyst crystals, supports the idea that

the diffusion of coke precursors out of the micropores is slower for the microporous catalysts owing to the longer diffusion paths, which ultimately result in faster coking [20, 25]. In agreement with the work by Rojo-Gama *et al.* [37], we suggest that coke species formed from methanol are accumulated in the micropores.

3.2.2. Influence on the product distribution

The influence of the post-synthetic treatments on the product distribution is given in this section. Previous MTH studies with H-ZSM-22 catalysts, conducted over a range of residence times, concluded that its shape selectivity is independent of the degree of coking and may be described solely as function of the conversion [7]. Accordingly, we will here examine the differences in product distribution for the microporous and hierarchical catalysts over the full range of conversion.

Overall, the product mixtures are very rich in C_{5+} alkenes, with a negligible content of aromatics, as illustrated by the representative chromatogram shown in Fig. S8 and selectivities displayed in Fig. 3a,b. This is in agreement with the typical product spectrum reported for the H-ZSM-22 catalyst [2, 7, 9, 10]. Hence, Figure 3c,d shows that the product yields were very similar for all the studied catalysts. The initial yields (at 100 % conversion) of C_{5+} olefins were > 42 %. The main by-products were C_3 and C_4 alkenes, and a very low amount of C_2 (< 5 %) was obtained. The C_{5+} hydrocarbon yield increased to a maximum at around 90 % conversion, while C_3 and C_4 yield decreased for all the catalysts with decreasing conversion. Clearly, the hierarchical materials yielded the highest C_{5+} fraction. Notably, the highest C_{5+} yield (58 %, *c*-ZSM-22-*ats1-HCl*, at XYZ % conversion) represents a significant improvement of 5 percentage points with respect to previously reported values for one-dimensional medium pore size zeolites [1, 6]. by.

The overall similarities of the product distributions of the microporous and hierarchical catalysts indicate that the product shape selectivity of the H-ZSM-22 catalysts in the MTH reaction is governed by the micropore system inherent of the TON topology, regardless of the introduction of mesopores, in agreement with Dyballa *et al.* [35]. Furthermore, we can speculate that reactions on acid sites at the external surface (pore mouths) are of little relevance, since these presumably would not be affected by steric restrictions and would result in a different (non selective) product distribution.

So, the effluent distribution is dictated by product shape selectivity. However, the transition shape selectivity may change for mesoporous catalysts. To evaluate this, more information can be extracted by analysing the C_3/C_2 ratio and the ethene to 2-methyl-2-butene (2M2B) ratios. Assuming that ethene originates mainly from the aromatic-based cycle in MTH [2, 38-41] and 2-methyl-2-butene (2M2B) and propene are to a large extent formed from the alkene methylation/cracking reactions operating in the olefin cycle [2, 40, 41], these ratios can be used to study the relative propagation of each of the mechanistic cycles. This analysis is based on the studies by Bhan *et al.* on MFI catalysts [42, 43]. Relative to ZSM-5, the alkene-based cycle is more pronounced for the TON topology [2, 10]. Therefore, ethene/2M2B ratios well below one and high C_3/C_2 ratios were expected.

Figure 4 shows the C_3/C_2 ratio (a-b) and the ethene/2M2B ratio (c-d) versus conversion for the commercial and lab-made catalysts, respectively. The latter plots are restricted to 40-100 % conversion range, in order to make the visual examination clearer. Generally, the hierarchical catalysts display a similar behaviour with conversion, with particular deviations for the some of the lab-made catalysts. The C_3/C_2 ratio increased drastically with deactivation up to a maximum at 45-55 % conversion for all the hierarchical catalysts, together with a more rapid drop of the ethene/2M2B ratio as compared with

the untreated catalyst. As exception, the *m*-ZSM-22-*tba1-HCl* catalyst exhibited a lower increase of the C_3/C_2 ratio and a reduced drop of the ethene/2M2B ratio for shorter reaction times, and the *m*-ZSM-22-*ast1-HCl* catalyst showed only a slight increase in the C_3/C_2 ratio with deactivation. Finally, the untreated *m*-ZSM-22 catalyst showed a continuous decreasing trend in C_3/C_2 ratio with deactivation and no appreciable variation of the ethene/2M2B ratio.

Mechanistic information can be extracted from the analysis of the variation of the C_3/C_2 and ethene/2M2B ratios together with the shape of the deactivation curves shown in Fig. 1. Firstly, the results indicate that ethene formation is more significant for the most rapidly deactivating catalysts (*c*-ZSM-22, *m*-ZSM-22 and *m*-ZSM-22-*ats1-HCl*), whereas the catalysts with higher stability (*c*-ZSM-22-*ats1-HCl* and *m*-ZSM-22-*at1-HCl*) showed a lower relative production of ethene and a higher contribution of propene and 2M2B products The general trend is that a more rapid loss of activityis associated with a higher production of ethene. With this information, we hypothesize a different degree of progression of alkene methylation and cracking reactions characteristic of the olefin cycle dominant over the H-ZSM-22 catalyst [10], which will also be further discussed in the next section. Clearly, the more stable catalysts allow a longer operation of the olefin cycle, leading to larger propene and higher alkenes production for longer times. When the maximum in the C_3/C_2 ratio is encountered (and the corresponding shallow minimum or stable final value of the ethene/2M2B ratio), the propagation of the alkene cycle is not increased anymore and a progressive drop in activity is observed until complete deactivation. The higher formation of ethene observed for the catalysts which deactivated faster, suggests a higher participation of the aromatic cycle already from short reaction times (*m*-ZSM-22 and *m*-ZSM-*22-ats1-HCl*) or after a short initial period of olefin cycle progression (*m*-ZSM-22-*tba1-HCl*). Together with the lower C_{5+}

contribution and the higher C_4-HTI (hydrogen transfer index-HTI is defined as the combined yields of isobutene and *n*-butane divided by the total yield of C_4 alkanes and alkenes) (Fig. S7), this suggests that product molecules cannot easily diffuse out of the 1-D microporous catalyst topology in these cases, and will be involved in aromatization and cyclization reactions (which involve ethene formation) leading to deactivation, together with methanol direct conversion into coke.

3.3. Elucidating the causes for the superior catalytic behaviour

The post-synthetic treatments modified the elemental composition, textural and acidity features of the studied catalyst, and these variations may affect the MTH activity and stability in an interdependent manner [12, 19-21, 23, 35, 44]. Therefore, sestablishing single-parameter correlations between characterization data nd the catalytic performance is not straightforward. All the commercial catalysts had very similar Si/Al ratios of 47-50, and all the lab-made catalysts showed Si/Al ratios of 34-39 (Table 1), both with similar acid strength (as seen with CO adsorption), meaning that variations in catalytic conversion are too large to be caused by a minor modification of the acid site density or acid strength for each series.

The optimization of an industrial catalytic operation focuses mainly on obtaining more amounts of the desired products per grams of catalyst used, which is determined by the total conversion capacity concept. It represents the total capacity of the catalyst for converting reactants into hydrocarbon products until complete loss of its activity. Given the small differences in acid site densities of the catalysts,the total methanol conversion capacity, was calculated as the total grams of methanol converted per gram of catalyst (g g^{-1}). These values were used to analyse the variations in catalytic performance in a quantitative manner (Fig. 5). The *c*-ZSM-22-*ats1-HCl* and *m*-ZSM-22-*at1-HCl* catalysts

showed the best catalytic performance, with an exceptional enhancement of the total conversion capacity up to the same value of 30 g g^{-1}.This represents a 10-fold increase for the commercial catalysts and an increment by a factor of 16.6 for the lab-made catalyst. Previous investigations with H-ZSM-22 catalysts with Si/Al ratio of 30 found that a maximum total conversion capacity of 12 g g^{-1} could be obtained when applying optimized reaction conditions [9]. Thus, the present data represent an improvement by 300 % [9].

For the *c*-ZSM-22 with 200 nm crystals (Fig.S2), the most beneficial treatment was the surfactant-assisted treatment followed by acid washing, which led to 2 nm sized mesopores. For the lab-made catalyst comprising thinner particles of less than 60 nm, the standard alkaline treatment with NaOH and sequential acid washing gave the greatest MTH catalytic performance. This treatment also caused the highest external and microporous surface area. The very different effects of the various treatments highlight again the importance of the physico-chemical properties of the starting material. Clearly, porosity and acidic properties cannot be discussed independently, since the acidity is useless if it is not accessible, and similarly, the porosity will not be fully effective if it does not provide access to reactive centers (e.g. closed mesopores).

Concentrating first on the textural properties, Fig. 6a shows the total methanol conversion capacity as a function of external surface area (S_{ext}) for all the studied catalysts. The *c*-ZSM-22 and *m*-ZSM-22 microporous catalysts displayed the lowest values for S_{ext}. For the commercial treated catalysts (open points), a rather linear correlation of the total conversion capacity with the S_{ext} was observed, indicating that the created intra-crystalline mesopores makes the acid sites more easily accessible for the reaction to occur. However, the sample with the highest methanol conversion capacity (*c*-ZSM-*22-ats1-HCl*) clearly deviates from the trend, showing a very low

mesopore surface area. This demonstrates that additional factors play a decisive role in determining the catalytic performance. For the lab-made treated catalysts (closed points), the total methanol conversion capacity varies hugely with only minor changes in S_{ext}. However, the correlation of conversion capacity with the internal surface area (S_{micro}) shown in Fig. 6b indicates that, in this case, the improvement in conversion capacity may be well explained by an increased microporosity. This indicates that both, mesoporosity and microporosity can contribute to improving the catalytic performance of ZSM-22 samples. The low conversion capacity for the *m*-ZSM-*22-ats1-HCl* catalyst was expected owing to the severe micropore blocking caused by non-acidic species (see complementary article).

Figure 7 shows the total methanol conversion capacity as a function of the amount of Brønsted (a) and Lewis (b) acid sites accessible to pyridine. It is important to note that the acid treated catalysts have acidic sites fully accessible to pyridine (Fig. S4), except for the *m*-ZSM-22 and *m*-ZSM-*22-ats1-HCl* catalysts, which showed a notable blocked access to the Brønsted acid sites (Fig. S4). Roughly, a linear correlation between the amount of accessible Brønsted acid sites and the total methanol conversion capacity was found for all the catalyst, except for the *c*-ZSM-*22-ats1-HCl* sample (Fig. 7a). The results imply that the increased catalytic performance resulted from increased population of accessible strong acid sites. However, it must be mentioned that the outlier is one of the best catalysts overall.

The concentration of the Lewis acid sites is systematically higher for the commercial treated catalysts with respect to the lab-made treated samples (Fig. 7b). The plots are separated in three regions, corresponding to the catalysts with high (top), moderate (middle) or low (bottom) methanol conversion capacity. Among the catalysts showing the best catalytic performance, the *c*-ZSM-22-*ats1-HCl* (open data point) sample

showed a marked contribution of LAS, whereas the amount of BAS was essentially unchanged. On the contrary, the lab-made *m*-ZSM-22-*at1-HCl* catalyst had a notable increase in BAS but a minor contribution of LAS, displaying the opposite trend. The catalysts in the middle region behave somehow similarly. In this case, however, the Brønsted acidity was increased for the commercial *c*-ZSM-22-*ats2-HCl* sample, accompanied by a marked contribution of LAS, whereas only the BAS of the lab-made treated catalyst (*c*-ZSM-22-*tba1-HCl*) catalyst were significantly increased. The commercial catalyst sample with the lowest increment in conversion capacity (*c*-ZSM-22-*tba2-HCl*) showed a combined contribution of Brønsted and Lewis acidity, but both lower than the rest of samples. As mentioned, the access to the BAS of the *m*-ZSM-22-*ats1-HCl* sample was hindered, which results in a substantially lower lifetime for this catalyst [45].

Overall, the results show that the post-synthetic treatments resulted in the enhancement of the catalytic performance for both of the microporous ZSM-22 starting catalysts, but the modifications of the porous and acidic properties were very different. The results led us to propose that the accessible BAS of the microporous *c*-ZSM-22 catalyst allow the initiation of the olefin cycle in this catalyst. Upon desilication, a higher diffusion of the higher alkenes caused by enhanced porous properties and increased concentration of Brønsted acid sites favours the alkene methylation/cracking reactions, resulting in increased conversion capacity. However, it also appears that the larger concentration of LAS contribute to increasing the catalytic performance. For the *m*-ZSM-22 catalyst, the restricted micropores resulted in a limited activity in the MTH conversion, but the increased microporosity and the resulting accessible BAS after treatment allow the propagation of the olefin cycle in the lab-made treated catalysts.

Even though the effect of LAS on the zeolite catalytic activity is not fully understood, a number of contributions proposed a synergistic effect between Lewis and nearby Brønsted acid sites lead to enhance the activity of acid catalytic reactions over zeolite catalysts [46, 47]. Increased activity in the MTH conversion has also been reported for desilicated ZSM-5 catalysts samples with higher Lewis acidity [20]. It has been proposed that LAS may promote hydrogen transfer reactions leading to the formation of formaldehyde from methanol, which further reacts with alkenes at the BAS to produce coke over ZSM-5 catalyst [48, 49]. Conversely, it has been reported that the incorporation of Ca into ZSM-5 leads to $CaOCaOH^+$ species with Lewis character that weaken the acid strength and cause reduction of hydride transfer reaction rate and consequently the suppression of the aromatic cycle and increasing light olefin selectivity [50]. The results here agree better with the latter idea, since the interaction of a bridging OH group with a Lewis site seems to promote the alkene cracking/methylation reactions, possibly because LAS are more prone to accept coke species leaving the BAS ready for operating the alkene cycle. However, since no significant difference in acid strength among the studied catalysts is found, this effect might play a minor role.

A previous kinetic study showed that it is the textural properties rather than modifications of the intrinsic reactivity of the active sites that dictate the catalytic behaviour of hierarchical catalysts [51]. Thiswas further examined by measuring the uptake of toluene at 100 °C (Fig. 8). In addition to the two microporous H-ZSM-22 catalysts, two representative samples were chosen: *c*-ZSM-22-*ats2-HCl* and *c*-ZSM-22-*tba2-HCl* for the commercial series and *m*-ZSM-22-*at1-HCl* and *m*-ZSM-22-*tba1-HCl* for the lab-made set. In principle, the toluene molecule (6.1 Å) would have difficulties to diffuse through the micropores of the H-ZSM-22 zeolite framework. This suggests

that the diffusion of the toluene molecule might be limited for the samples with micropores only. Figure 8a clearly shows a higher adsorption capacity for the hierarchical catalysts as compared with the commercial microporous materials. Since the micropore volumes of the catalysts were practically unaffected by the treatments, the higher adsorption capacity may be attributed to the increased external (and thus total) pore volume, an improved accessibility and/or shorter diffusion path lengths for the mesoporous crystals. A reduction of the concentration of EFAl species after the acid washing might also contribute to improve the diffusivity of the hierarchical catalysts [52]. The toluene uptake for the lab-made hierarchical catalysts correlates with the increased total conversion capacity (Fig. 5b), suggesting that, in this case, the micropore volume was fully accessible. The diffusivity of the lab-made catalyst was barely increased by the post-synthetic treatments, as deduced from the slightly steeper slope of the adsorption curve at short times. It should be mentioned that the uptake experiments were carried out at conditions far from the actual reaction temperature and pressures, implying that the diffusion of toluene will be different in the two cases..Nevertheless, the total uptake capacities are considered relevant for the study.

4. Conclusions

In the present study, a series of microporous/mesoporous catalysts resulting from three different desilication treatments *i.e.* NaOH treatment, treatment using mixtures of NaOH with CTAB, and treatment using mixtures of NaOH with TBAOH, always followed by sequential acid leaching with two different microporous H-ZSM-22 starting materials were tested in the conversion of methanol to hydrocarbons. A significant enhancement of the H-ZSM-22 catalytic lifetime was obtained for the hierarchical catalysts. However, it turned out that the effects of the post-synthetic treatments varied

strongly depending on the starting material. Further, the improvements in catalyst performance were caused by alterations of different catalyst properties for the two starting materials. For the commercial material, the total methanol conversion was increased at most by a factor of 10 after the combined alkaline and CTAB treatment followed by acid washing A 17-fold increase was achieved for the lab-made catalysts treated with NaOH and then acid washed. The high selectivity towards the aromatic-free C_{5+} alkene fraction was slightly enhanced after the post-synthetic treatments, reaching a maximum yield of 58 % of products in this fraction.

The hierarchical catalysts solved the limitations of the solely microporous H-ZSM-22 catalyst. The correlations between the porous and acidic modifications and the total conversion capacity led us to propose that the treatments lead to a more efficient use of the hierarchical commercial catalyst particle, which has crystals of 200 nm in thickness. This is the result of a synergetic effect of mesopore formation, enhanced accessibility to the acid sites, and increased adsorption and transport properties. The presence of Lewis acidity was also shown to have a beneficial effect on the conversion capacity in this case. The catalytic improvements seen for the lab-made catalyst having thinner needle-shaped crystals were mainly caused by an enhanced accessibility to the micropore volume and consequently to the Brønsted acid sites. We hypothesize that the improved catalyst properties of the hierarchical materials allow a longer propagation of the olefin cycle with reaction time. The olefin cycle is the active mechanistic cycle operating for the TON topology, thus resulting in the improvement of the catalytic performance.

The present study demonstrates the substantial improvements in the catalyst performance in the MTH reaction of H-ZSM-22 catalysts that can be achieved by different desilication methods followed by sequential acid washing.t. In terms of commercial or pilot plant scale operation, the use of the hierarchical H-ZSM-22

catalysts will lead to less frequent regeneration and might allow regular fixed bed operation, thereby significantly lowering process investments and operation costs. Furthermore, the strategies carried out in this work could also be extended to improve catalytic performance of other one dimensional 10-ring topologies.

Acknowledgements

This publication is part of the inGAP Centre of research-based Innovation, which receives financial support from the Norwegian Research Council under contract no. 174893.

Table 1

Composition, acidity and textural properties of the studied samples.

Sample	Si/Al[a] (mol mol^{-1})	Acid sites[b] (µmol g^{-1})		Pore volume (cm^3 g^{-1})		Surface area (m^2 g^{-1})	
		c_{BAS}	c_{LAS}	V_{micro}[c]	V_{ext}	S_{total}[d]	S_{ext}[c]
c-ZSM-22	49	240	30	0.08	0.07	232	33
c-ZSM-22-*at1-HCl*	48	-	-	0.08	0.48	276	82
c-ZSM-22-*ats1-HCl*	50	220	100	0.08	0.21	257	58
c-ZSM-22-*ats2-HCl*	48	310	90	0.07	0.45	296	114
c-ZSM-22-*tba2-HCl*	47	280	70	0.09	0.20	272	44
m-ZSM-22	38	240	30	0.05	0.34	163	26
m-ZSM-22-*at1-HCl*	36	380	50	0.08	0.48	236	39
m-ZSM-22-*ats1-HCl*	34	210	50	0.03	0.20	108	29
m-ZSM-22-*tba1-HCl*	39	370	40	0.08	0.34	213	21

[a]From elemental analysis

[b]Amount of Brønsted or Lewis acid sites determined by IR spectroscopy of adsorbed pyridine.

[c] from *t*-plot method. V_{ext} and S_{ext} represent the pore volume and surface area for all the pores except the micropores.

[d] Total surface area using BET method.

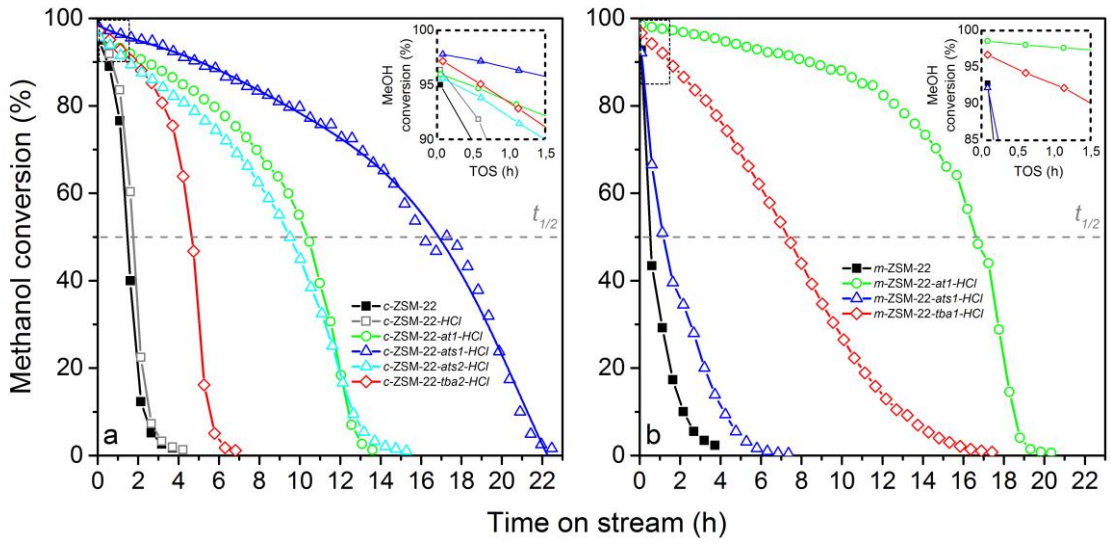

Fig. 1. Methanol conversion versus time on stream for the parent and treated commercial (**a**) and in lab-made (**b**) ZSM-22 zeolite catalysts, at WHSV = 2 h^{-1} and T = 400 ºC. $t_{1/2}$ indicates the time at which the conversion decreased by 50%.

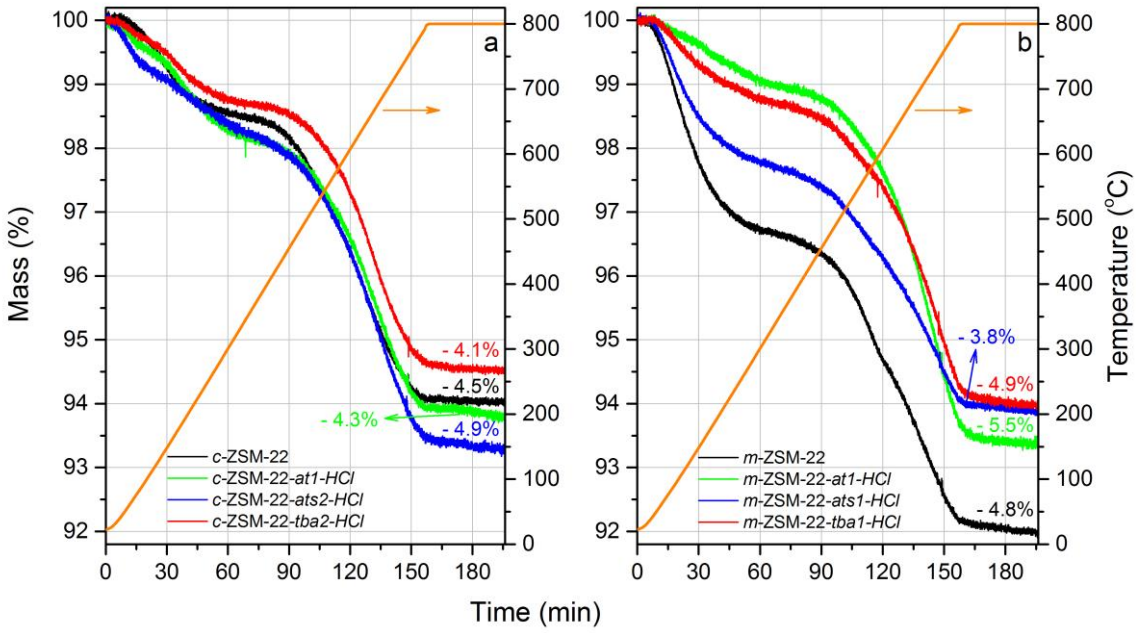

Fig. 2. TGA measurements of the spent commercial (**a**) and lab-made (**b**) untreated and hierarchical catalysts. Numbers show the mass loss (%) of deactivated catalysts during coke combustion, after removing water (normalized to the second drop of the curve).

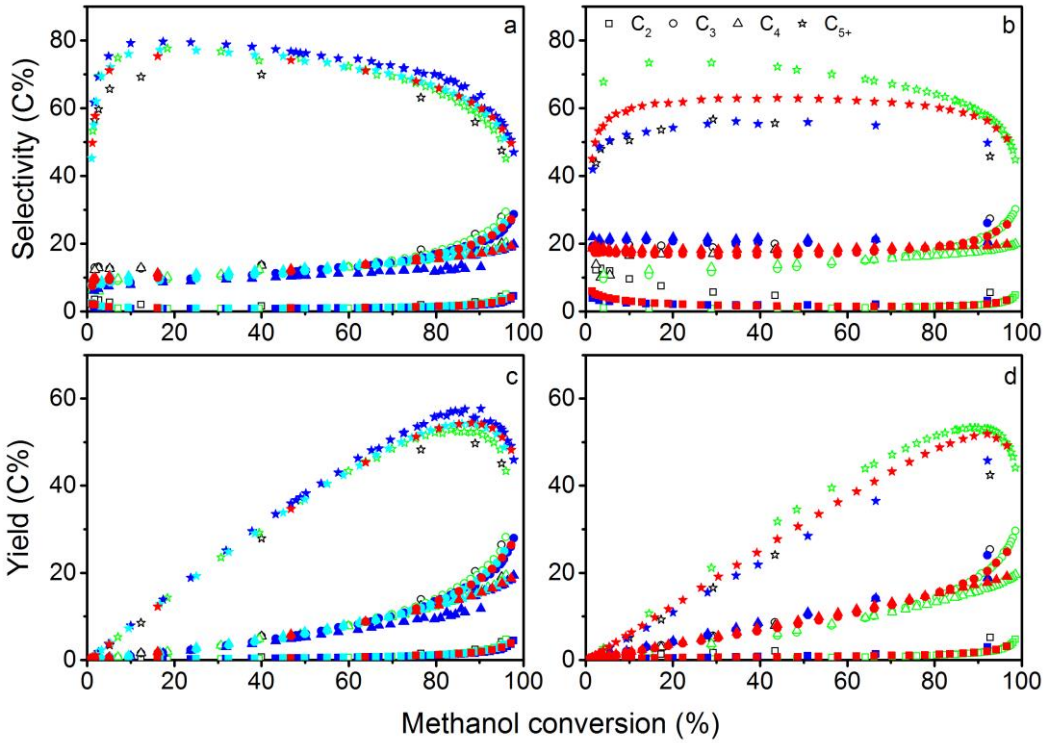

Fig. 3. Product selectivity and yield as a function of methanol conversion for the parent and treated commercial (**a and c**) and lab-made (**b and d**) H-ZSM-22 catalysts, at WHSV = 2 h^{-1} and T = 400 ºC. *c*- and *m*-ZSM-22-*at1-HCl* are shown in green, *c*- and *m*-ZSM-22-*ats1-HCl* in blue and *c*-ZSM-*22-ats2-HCl* in light blue, *c*-ZSM-22-*tba2-HCl* and *m*-ZSM-22-*HCl* in red. Untreated catalysts are shown in black.

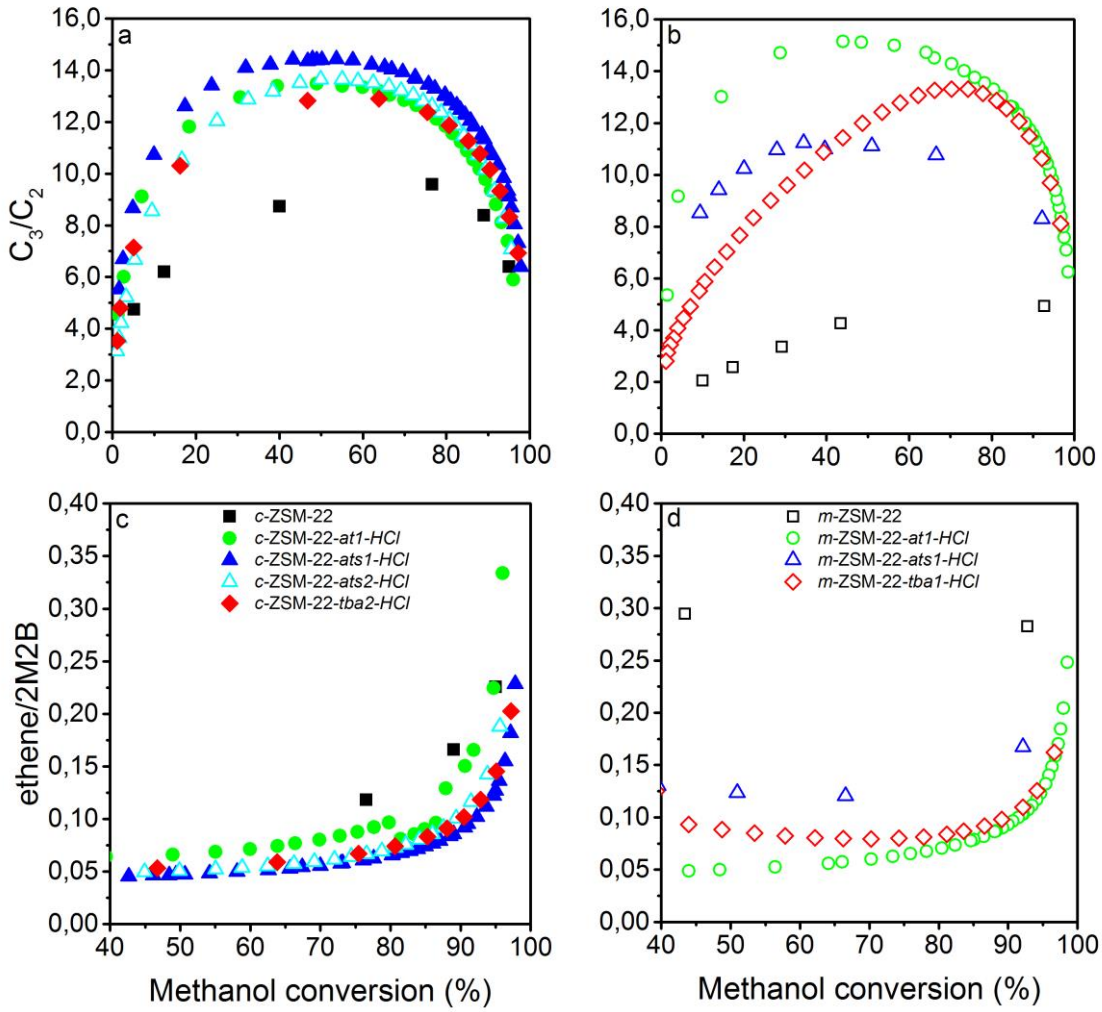

Fig. 4. C_3/C_2 (**top panels**) and ethene/2-methyl-2-butene (**bottom panels**) yield ratio as a function of methanol conversion over the parent and treated commercial (**a and c**) and lab-made (**b and d**) H-ZSM-22 catalysts, at WHSV = 2 h^{-1} and T = 400 ºC.

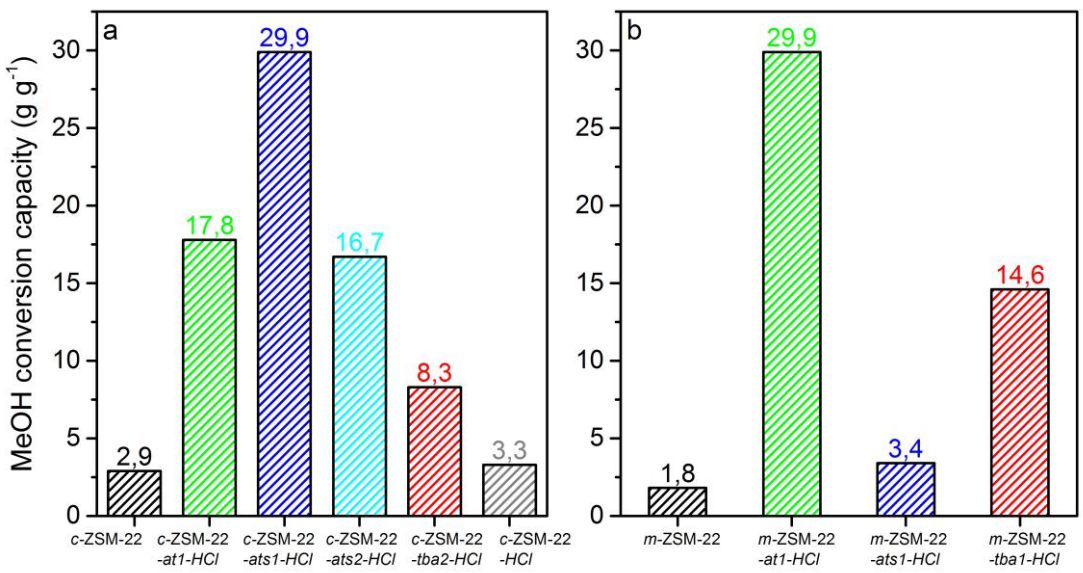

Fig. 5. Calculated total methanol conversion capacity for the (**a**) commercial treated samples and (**b**) lab-made treated catalysts.

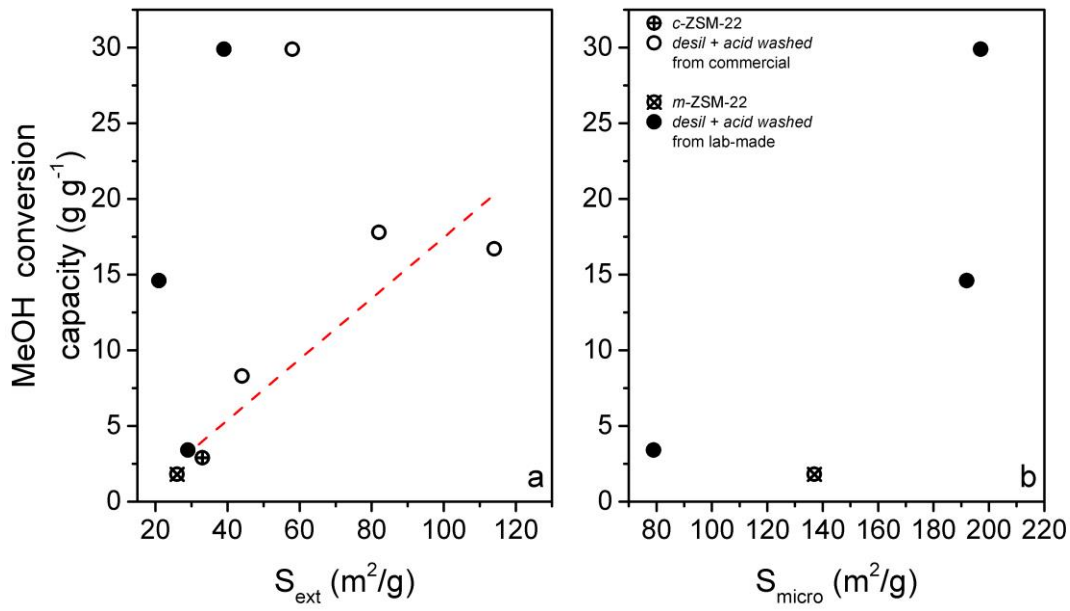

Fig. 6. Correlation of total methanol conversion capacity with the external surface area (S_{ext}) in panel **a** and with the microporous surface area (S_{micro}) in panel **b**, for the studied catalysts.

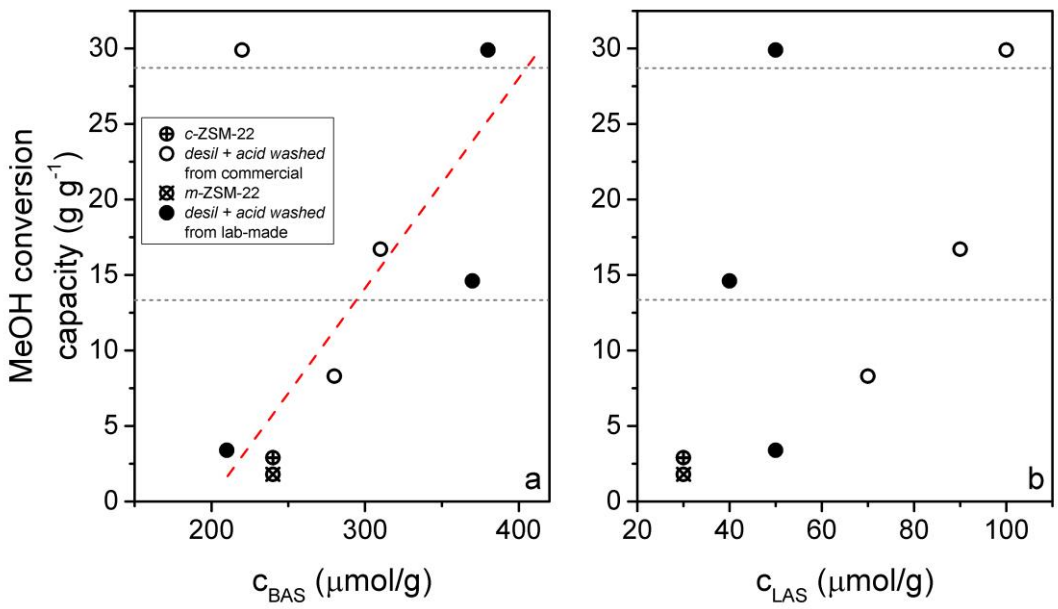

Fig. 7. Correlation of total methanol conversion capacity with the amount of accessible Brønsted acid sites (c_{BAS}) in panel **a** and Lewis acid sites (c_{LAS}) in panel **b**, for the studied catalysts.

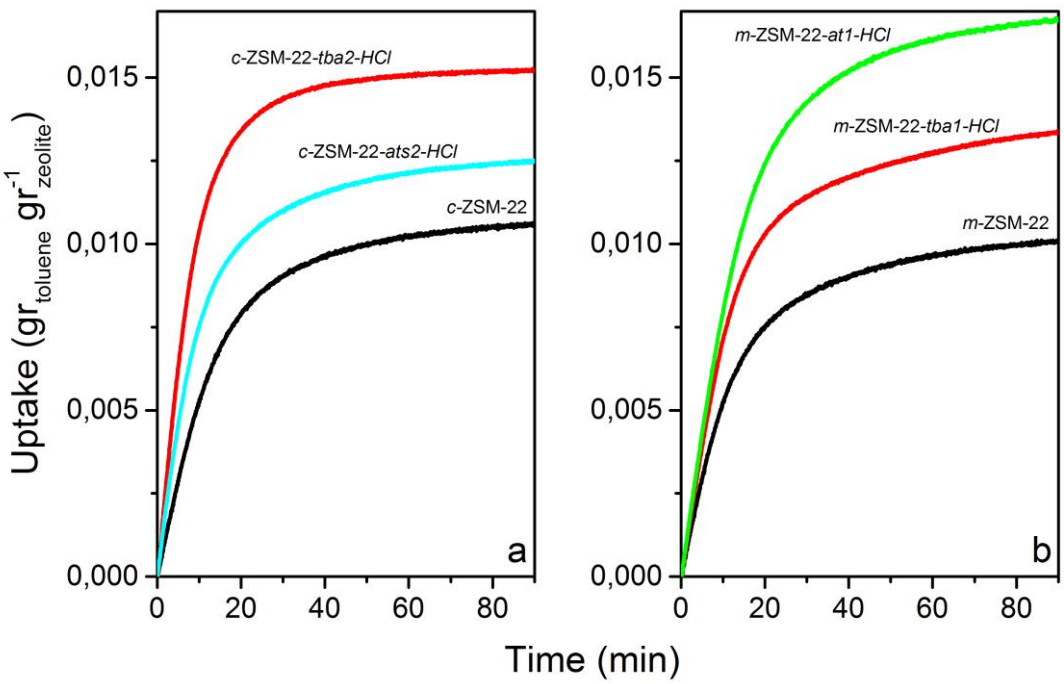

Fig. 8. Toluene uptake curves of the selected parent and hierarchical commercial (**a**) and lab-made (**b**) H-ZSM-22 catalysts.

References

[1] M.W. Erichsen, J.S. Martinez-Espin, F. Joensen, S. Teketel, P. del Campo Huertas, K.P. Lillerud, S. Svelle, P. Beato, U. Olsbye, 14 Syngas to Liquids via Oxygenates, Small-Scale Gas to Liquid Fuel Synthesis, (2015) 441.

[2] U. Olsbye, S. Svelle, M. Bjorgen, P. Beato, T.V.W. Janssens, F. Joensen, S. Bordiga, K.P. Lillerud, Conversion of Methanol to Hydrocarbons: How Zeolite Cavity and Pore Size Controls Product Selectivity, Angew. Chem., Int. Ed., 51 (2012) 5810-5831.

[3] M. Stocker, Methanol-to-hydrocarbons: catalytic materials and their behavior, Microporous Mesoporous Mater., 29 (1999) 3-48.

[4] N.A. Owen, O.R. Inderwildi, D.A. King, The status of conventional world oil reserves—Hype or cause for concern?, Energy Policy, 38 (2010) 4743-4749.

[5] B. Smit, T.L.M. Maesen, Towards a molecular understanding of shape selectivity, Nature, 451 (2008) 671-678.

[6] S. Teketel, M.W. Erichsen, F.L. Bleken, S.S.K.P. Lillerud, U. Olsbye, Shape selectivity in zeolite catalysis. The methanol to hydrocarbons (MTH) reaction, Catalysis, 26 (2014) 179-217.

[7] S. Teketel, W. Skistad, S. Benard, U. Olsbye, K.P. Lillerud, P. Beato, S. Svelle, Shape Selectivity in the Conversion of Methanol to Hydrocarbons: The Catalytic Performance of One-Dimensional 10-Ring Zeolites: ZSM-22, ZSM-23, ZSM-48, and EU-1, ACS Catal., 2 (2012) 26-37.

[8] G.T. Kokotailo, J.L. Schlenker, F.G. Dwyer, E.W. Valyocsik, The framework topology of ZSM-22: a high-silica zeolite, Zeolites, 5 (1985) 349-351.

[9] S. Teketel, S. Svelle, K.-P. Lillerud, U. Olsbye, Shape-selective conversion of methanol to hydrocarbons over 10-ring unidirectional-channel acidic H-ZSM-22, ChemCatChem, 1 (2009) 78-81.

[10] S. Teketel, U. Olsbye, K.-P. Lillerud, P. Beato, S. Svelle, Selectivity control through fundamental mechanistic insight in the conversion of methanol to hydrocarbons over zeolites, Microporous Mesoporous Mater., 136 (2010) 33-41.

[11] J. Li, Y. Wei, Y. Qi, P. Tian, B. Li, Y. He, F. Chang, X. Sun, Z. Liu, Conversion of methanol over H-ZSM-22: The reaction mechanism and deactivation, Catal. Today, 164 (2011) 288-292.

[12] M.S. Holm, E. Taarning, K. Egeblad, C.H. Christensen, Catalysis with hierarchical zeolites, Catalysis Today, 168 (2011) 3-16.

[13] K. Na, M. Choi, R. Ryoo, Recent advances in the synthesis of hierarchically nanoporous zeolites, Microporous and Mesoporous Materials, 166 (2013) 3-19.

[14] M. Hartmann, Hierarchical zeolites: A proven strategy to combine shape selectivity with efficient mass transport, Angew. Chem., Int. Ed., 43 (2004) 5880-5882.

[15] K. Li, J. Valla, J. Garcia-Martinez, Realizing the commercial potential of hierarchical zeolites: new opportunities in catalytic cracking, ChemCatChem, 6 (2014) 46-66.

[16] S. Mitchell, A.B. Pinar, J. Kenvin, P. Crivelli, J. Karger, J. Perez-Ramirez, Structural analysis of hierarchically organized zeolites, Nat. Commun., 6 (2015) 8633.

[17] K. Na, G. Somorjai, Hierarchically Nanoporous Zeolites and Their Heterogeneous Catalysis: Current Status and Future Perspectives, Catal Lett, 145 (2015) 193-213.

[18] J. Shi, Y. Wang, W. Yang, Y. Tang, Z. Xie, Recent advances of pore system construction in zeolite-catalyzed chemical industry processes, Chem. Soc. Rev., 44 (2015) 8877-8903.
[19] D. Verboekend, J. Perez-Ramirez, Design of hierarchical zeolite catalysts by desilication, Catal. Sci. Technol., 1 (2011) 879-890.
[20] M. Bjoergen, F. Joensen, H.M. Spangsberg, U. Olsbye, K.-P. Lillerud, S. Svelle, Methanol to gasoline over zeolite H-ZSM-5: Improved catalyst performance by treatment with NaOH, Appl. Catal., A, 345 (2008) 43-50.
[21] F.L. Bleken, K. Barbera, F. Bonino, U. Olsbye, K.P. Lillerud, S. Bordiga, P. Beato, T.V.W. Janssens, S. Svelle, Catalyst deactivation by coke formation in microporous and desilicated zeolite H-ZSM-5 during the conversion of methanol to hydrocarbons, J. Catal., 307 (2013) 62-73.
[22] F. Schmidt, C. Hoffmann, F. Giordanino, S. Bordiga, P. Simon, W. Carrillo-Cabrera, S. Kaskel, Coke location in microporous and hierarchical ZSM-5 and the impact on the MTH reaction, J. Catal., 307 (2013) 238-245.
[23] F. Schmidt, M.R. Lohe, B. Buechner, F. Giordanino, F. Bonino, S. Kaskel, Improved catalytic performance of hierarchical ZSM-5 synthesized by desilication with surfactants, Microporous Mesoporous Mater., 165 (2013) 148-157.
[24] M. Choi, K. Na, J. Kim, Y. Sakamoto, O. Terasaki, R. Ryoo, Stable single-unit-cell nanosheets of zeolite MFI as active and long-lived catalysts, Nature (London, U. K.), 461 (2009) 246-249.
[25] J. Kim, M. Choi, R. Ryoo, Effect of mesoporosity against the deactivation of MFI zeolite catalyst during the methanol-to-hydrocarbon conversion process, Journal of Catalysis, 269 (2010) 219-228.
[26] C. Mei, P. Wen, Z. Liu, H. Liu, Y. Wang, W. Yang, Z. Xie, W. Hua, Z. Gao, Selective production of propylene from methanol: Mesoporosity development in high silica HZSM-5, J. Catal., 258 (2008) 243-249.
[27] J. Perez-Ramirez, C.H. Christensen, K. Egeblad, C.H. Christensen, J.C. Groen, Hierarchical zeolites: enhanced utilisation of microporous crystals in catalysis by advances in materials design, Chem. Soc. Rev., 37 (2008) 2530-2542.
[28] L. Sommer, D. Mores, S. Svelle, M. Stoecker, B.M. Weckhuysen, U. Olsbye, Mesopore formation in zeolite H-SSZ-13 by desilication with NaOH, Microporous Mesoporous Mater., 132 (2010) 384-394.
[29] S. Liu, J. Ren, H. Zhang, E. Lv, Y. Yang, Y.-W. Li, Synthesis, characterization and isomerization performance of micro/mesoporous materials based on H-ZSM-22 zeolite, J. Catal., 335 (2016) 11-23.
[30] J.A. Martens, D. Verboekend, K. Thomas, G. Vanbutsele, J. Perez-Ramirez, J.-P. Gilson, Hydroisomerization and hydrocracking of linear and multibranched long model alkanes on hierarchical Pt/ZSM-22 zeolite, Catal. Today, Ahead of Print.
[31] P. Matias, C.C. Sa, I. Graca, J.M. Lopes, A.P. Carvalho, R.F. Ramoa, M. Guisnet, Desilication of a TON zeolite with NaOH: Influence on porosity, acidity and catalytic properties, Appl. Catal., A, 399 (2011) 100-109.
[32] C. Sá Couto, P. Matias, E.T. Santos, A. Fernandes, I. Graça, J.M. Lopes, M.F. Ribeiro, Towards a Deep Desilication/Dealumination of NU-10 Zeolite: Shape-Selectivity Regulation, European Journal of Inorganic Chemistry, 2012 (2012) 4190-4199.
[33] D. Verboekend, K. Thomas, M. Milina, S. Mitchell, J. Perez-Ramirez, J.-P. Gilson, Towards more efficient monodimensional zeolite catalysts: n-alkane hydro-isomerisation on hierarchical ZSM-22, Catal. Sci. Technol., 1 (2011) 1331-1335.

[34] P. del Campo, W.A. Slawinski, R. Henry, M.W. Erichsen, S. Svelle, P. Beato, D. Wragg, U. Olsbye, Time- and space-resolved high energy operando X-ray diffraction for monitoring the methanol to hydrocarbons reaction over H-ZSM-22 zeolite catalyst in different conditions, Surf. Sci., 648 (2016) 141-149.
[35] M. Dyballa, U. Obenaus, M. Rosenberger, A. Fischer, H. Jakob, E. Klemm, M. Hunger, Post-synthetic improvement of H-ZSM-22 zeolites for the methanol-to-olefin conversion, Microporous Mesoporous Mater., 233 (2016) 26-30.
[36] U. Olsbye, S. Svelle, K.P. Lillerud, Z.H. Wei, Y.Y. Chen, J.F. Li, J.G. Wang, W.B. Fan, The formation and degradation of active species during methanol conversion over protonated zeotype catalysts, Chem. Soc. Rev., (2015) Ahead of Print.
[37] D. Rojo-Gama, S. Etemadi, E. Kirby, K.P. Lillerud, P. Beato, S. Svelle, U. Olsbye, Time- and space-resolved study of the Methanol to Hydrocarbons (MTH) reaction - influence of zeolite topology on deactivation patterns, Faraday Discuss., (2016) Ahead of Print.
[38] S. Svelle, F. Joensen, J. Nerlov, U. Olsbye, K.-P. Lillerud, S. Kolboe, M. Bjorgen, Conversion of Methanol into Hydrocarbons over Zeolite H-ZSM-5: Ethene Formation Is Mechanistically Separated from the Formation of Higher Alkenes, J. Am. Chem. Soc., 128 (2006) 14770-14771.
[39] M. Bjorgen, S. Svelle, F. Joensen, J. Nerlov, S. Kolboe, F. Bonino, L. Palumbo, S. Bordiga, U. Olsbye, Conversion of methanol to hydrocarbons over zeolite H-ZSM-5: On the origin of the olefinic species, J. Catal., 249 (2007) 195-207.
[40] M. Bjoergen, F. Joensen, K.-P. Lillerud, U. Olsbye, S. Svelle, The mechanisms of ethene and propene formation from methanol over high silica H-ZSM-5 and H-beta, Catal. Today, 142 (2009) 90-97.
[41] S. Svelle, U. Olsbye, F. Joensen, M. Bjorgen, Conversion of methanol to alkenes over medium- and large-pore acidic zeolites: steric manipulation of the reaction intermediates governs the ethene/propene product selectivity, J. Phys. Chem. C, 111 (2007) 17981-17984.
[42] S. Ilias, R. Khare, A. Malek, A. Bhan, A descriptor for the relative propagation of the aromatic- and olefin-based cycles in methanol-to-hydrocarbons conversion on H-ZSM-5, J. Catal., 303 (2013) 135-140.
[43] R. Khare, D. Millar, A. Bhan, A mechanistic basis for the effects of crystallite size on light olefin selectivity in methanol-to-hydrocarbons conversion on MFI, J. Catal., 321 (2015) 23-31.
[44] M. Milina, S. Mitchell, N.-L. Michels, J. Kenvin, J. Perez-Ramirez, Interdependence between porosity, acidity, and catalytic performance in hierarchical ZSM-5 zeolites prepared by post-synthetic modification, J. Catal., 308 (2013) 398-407.
[45] D. Verboekend, A.M. Chabaneix, K. Thomas, J.-P. Gilson, J. Perez-Ramirez, Mesoporous ZSM-22 zeolite obtained by desilication: peculiarities associated with crystal morphology and aluminum distribution, CrystEngComm, 13 (2011) 3408-3416.
[46] S. Li, A. Zheng, Y. Su, H. Zhang, L. Chen, J. Yang, C. Ye, F. Deng, Bronsted/Lewis Acid Synergy in Dealuminated HY Zeolite: A Combined Solid-State NMR and Theoretical Calculation Study, J. Am. Chem. Soc., 129 (2007) 11161-11171.
[47] C.J.A. Mota, D.L. Bhering, N. Rosenbach, Jr., A DFT study of the acidity of ultrastable Y zeolite: Where is the Bronsted/Lewis acid synergism?, Angew. Chem., Int. Ed., 43 (2004) 3050-3053.
[48] M.S. Holm, S. Svelle, F. Joensen, P. Beato, C.H. Christensen, S. Bordiga, M. Bjorgen, Assessing the acid properties of desilicated ZSM-5 by FTIR using CO and 2,4,6-trimethylpyridine (collidine) as molecular probes, Appl. Catal., A, 356 (2009) 23-30.

[49] S. Müller, Y. Liu, F.M. Kirchberger, M. Tonigold, M. Sanchez-Sanchez, J.A. Lercher, Hydrogen transfer pathways during zeolite catalyzed methanol conversion to hydrocarbons, Journal of the American Chemical Society, (2016).
[50] I. Yarulina, S. Bailleul, A. Pustovarenko, J.R. Martinez, K.D. Wispelaere, J. Hajek, B.M. Weckhuysen, K. Houben, M. Baldus, V. Van Speybroeck, Suppression of the Aromatic Cycle in Methanol-to-Olefins Reaction over ZSM-5 by Post-Synthetic Modification Using Calcium, ChemCatChem, 8 (2016) 3057-3063.
[51] I. Hill, A. Malek, A. Bhan, Kinetics and Mechanism of Benzene, Toluene, and Xylene Methylation over H-MFI, ACS Catal., 3 (2013) 1992-2001.
[52] K.A. Tarach, J. Martinez-Triguero, F. Rey, K. Góra-Marek, Hydrothermal stability and catalytic performance of desilicated highly siliceous zeolites ZSM-5, Journal of Catalysis, 339 (2016) 256-269.